Open Access

Fiber In-Line Fabry-Perot Interferometer With Offset Splicing for Strain Measurement With Enhanced Sensitivity
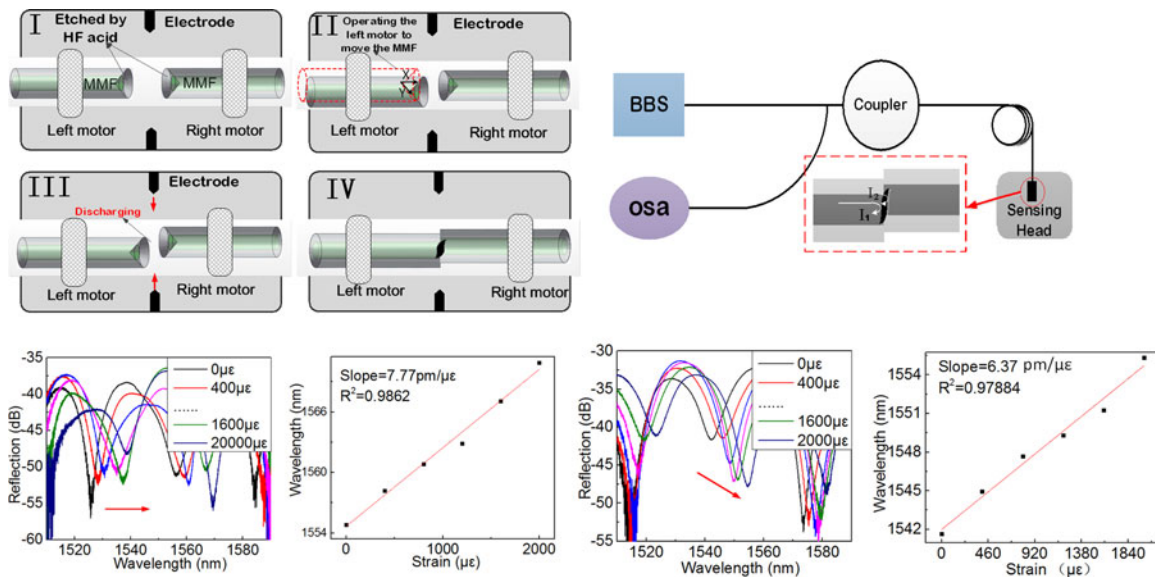
Ye Liu
D. N. Wang, *Senior Member, IEEE*

Fiber In-Line Fabry-Perot Interferometer With Offset Splicing for Strain Measurement With Enhanced Sensitivity

Ye Liu and D. N. Wang, *Senior Member, IEEE*

College of Optical and Electronic Technology, China Jiliang University,
Hangzhou 310018, China

Abstract: We demonstrate a Fabry–Perot interferometer with inner air-cavity for ultrasensitive strain measurement. The device is fabricated by fusion splicing of two sections of etched multimode fiber with offset. By selecting the appropriate value of the offset, the strain sensitivity can be greatly increased. In the case of introducing two-dimensional offset, the strain sensitivity can be increased by more than 4.5 pm/$\mu\varepsilon$ when compared with that without offset. The device is simple in fabrication, robust in structure, economic in cost, and convenient in operation, and has high potential in many strain sensing applications.

Index Terms:

1. Introduction

Optical fiber strain sensors have many applications in civil engineering and aerospace industry. One of the widely used optical fiber strain sensors at present is based on Fabry-Perot (FP) cavity, due to its simple configuration, compact size, easy fabrication, excellent stability and good sensitivity [1]–[15]. The optical fiber FP interferometer sensors can be divided into two types: extrinsic and intrinsic [8]–[10]. Although the extrinsic FP interferometer (EFPI) is simple in fabrication and low in temperature cross-sensitivity, it has relatively weak interference signal and needs careful system alignment. The problems of EFPI can be effectively overcome by use of intrinsic FP interferometer (IFPI) and in addition, by adopting fiber inner air-cavity in the IFPI, a low temperature cross-sensitivity can also be achieved [7], [11]–[12]. Many efforts have been made to enhance the strain sensitivity of IFPI based on inner air-cavity, such as the use of short cavity length [12], [13], small cavity wall thickness [14], or a thin crescent cavity shape [15]. However, such devices are poor in robustness, difficult in precise fabrication or not cost effective. Moreover, an ultra-short cavity length corresponds to a large free spectral range (FSR) in the output spectrum of the device, which may lead to that the fringe peak or dip goes beyond the wavelength range of the light source used and thus creating difficulties in performing the experiment.

In this Paper, we propose and demonstrate an optical fiber FP interferometer (FPI) sensor for highly sensitive strain measurement. The FPI is based on inner air-cavity fabricated by fusion splicing of two sections of etched multimode fiber (MMF) with offset and hence is simple fabrication,
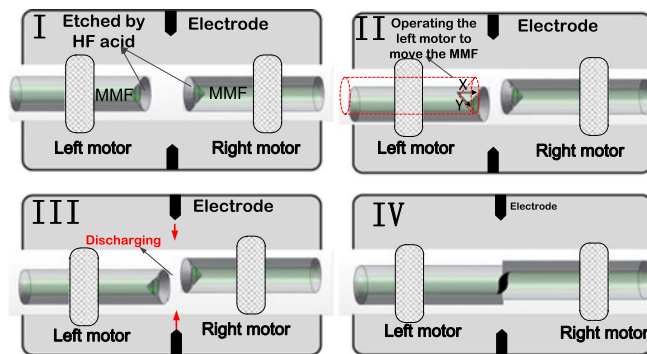
Fig. 1. Schematic diagram of the proposed FP cavity device fabrication process.
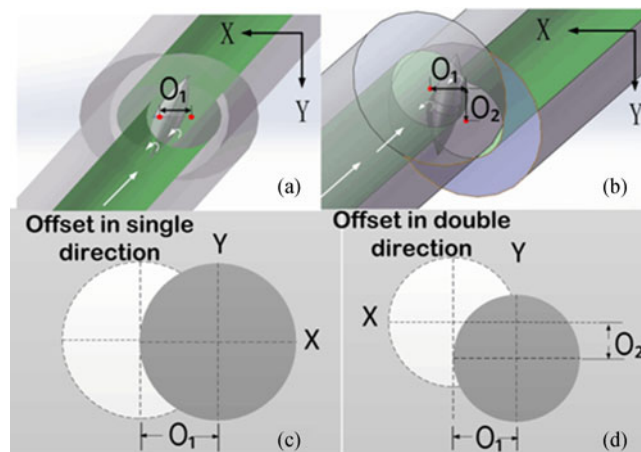

Fig. 2. (a) Schematic of the optical fiber FP cavity formed by fusion splicing two etched MMF with offsets. (b) Fiber end view of the two MMF with offset in X axis direction. (c) Fiber end view of the two MMF with offset in both X axis and Y axis directions.

robust in structure and economic in cost. By selecting the appropriate value of the offset, the strain sensitivity can be greatly increased. For instance, for an air-cavity length of $\sim$60.6 μm, the largest strain sensitivity achieved is 7.77 pm/$\mu\varepsilon$, compared with 3.26 pm/$\mu\varepsilon$, with inner air-cavity length of $\sim$64.6 μm, without offset.

2. Device Fabrication and Operating Principle

The proposed FP cavity device is fabricated by fusion splicing of two sections of etched MMF with offset. The fabrication process of the device with offsets in single or double directions are shown in Fig. 1.

1) A section of cleaved end of MMF is placed in hydrofluoric (HF) acid of 40% concentration for 4 minutes to create a tapered cavity at the fiber end.
2) The two sections of MMF with etched fiber end are placed in a fusion splicer, and then operating the left motor to introduce single or double direction movement of one section of MMF with accurate distance control.
3) The etched MMFs with offset are fusion spliced to form an irregular shaped inner air FP cavity.

During the device fabrication process, the discharge time and power employed in the fusion splicer (Fujikura 80s) are 300 ms and 50 bit respectively.

The schematic of the optical fiber FP cavity formed by fusion splicing of two etched MMF with offsets is shown in Fig. 2(a) and (b), where O_1 represents the offset value in X axis direction, and O_2
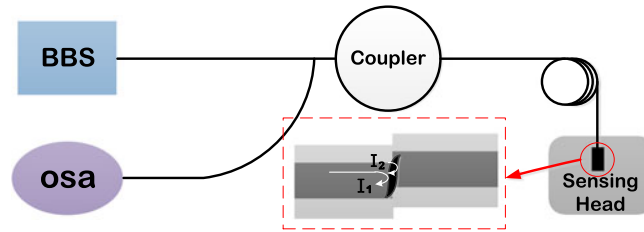
Fig. 3. Experimental setup for strain measurement. The inset shows the schematic diagram of the fiber FP cavity device.

denotes the offset value in Y axis. Fig. 2(c) and (d) demonstrate the fiber end view of the two MMF with offset in single direction (X axis direction) and double directions (X axis and Y axis directions) respectively. The incident light beam traveling along the fiber core of MMF is reflected by the two surfaces of the FP cavity respectively and the two reflected light beams are recombined in the fiber core, resulting in an interference fringe pattern at the output.

Assuming that the light intensities of the reflected beams by the two surfaces of the FP cavity are I_1 and I_2, respectively, the interference signal intensity can be written as:

$$I = I_1 + I_2 + 2\sqrt{I_1 I_2}\cos\left(\frac{4\pi nL}{\lambda} + \varphi_0\right) \tag{1}$$

where λ is the wavelength of the incident light, n is the refractive index (RI) of the cavity medium, L is cavity length and φ_0 is the initial phase of the interference. At the output fringe dip positions, the phase difference of the two reflected light beams satisfies the condition,

$$\frac{4\pi nL}{\lambda_m} + \varphi_0 = (2m + 1)\pi \tag{2}$$

where m is an integer, λ_m is the wavelength of the mth order interference dip. For the sake of simplicity, assuming that $\varphi_0 = 0$, then the intensity dip appears at the wavelength

$$\lambda_{dip} = \frac{4nL}{2m + 1} \tag{3}$$

The free spectral range in the spectrum can then be written as

$$\Delta\lambda = \frac{\lambda^2}{2nL} \tag{4}$$

For an air cavity, n = 1, the dip wavelength shift due to the axial strain can be derived as

$$\delta\lambda_{dip} = \frac{4\delta L}{2m + 1} \tag{5}$$

where $\delta\lambda$ is the change of air cavity length.

3. Experiment and Discussion

The experimental setup for strain test of our proposed device is shown in Fig. 3. The output from a broadband (BBS) light source is introduced to the fiber FP cavity device by a coupler and the reflected light beams are received by an optical spectrum analyzer (OSA) (YOKOGAWA 6390) with the resolution of 0.02 nm to record the spectrum. The wavelength range of the BBS is between 1452 and 1652 nm.

Fig. 4 shows the microscope image of a fiber FP cavity device sample without offset. The cavity length of the device sample is measured as ~64.6 μm.
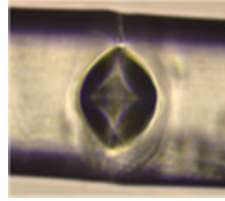
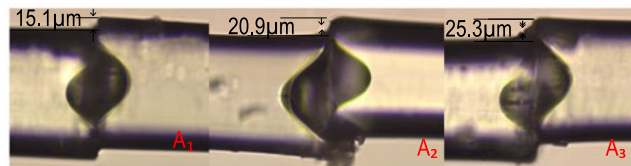Fig. 4. Microscope image of the device sample without offset.

Fig. 5. The microscope images of the fiber FP cavity device samples with different offsets in single direction. The offsets are ∼15.1, ∼20.9 and ∼25.3 respectively, and the corresponding air-cavity length are ∼62.5, ∼61.2 and ∼60.7 μm, respectively.
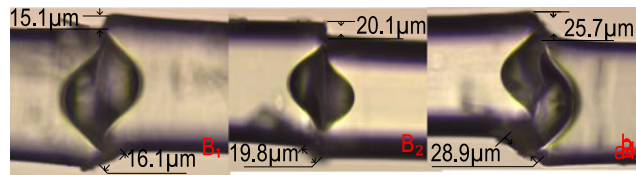

Fig. 6. The microscope images of the fiber FP cavity device samples with different offsets in double directions. The offsets values for X-axis and Y-axis directions, expressed as (x, y), are (15.1, 16.1), (20.1, 19.8) and (25.7, 28.9) respectively, and the corresponding air-cavity length are ∼62.9, ∼61.2 and ∼60.6 μm, respectively.

The microscope images of the fiber FP cavity device samples with different offsets in single direction are displayed in Fig. 5. The offsets are ∼15.1, ∼20.9 and ∼25.3 μm respectively, and the corresponding air-cavity lengths are ∼62.5, ∼61.2 and ∼60.7 μm, respectively.

The microscope images of the fiber FP cavity device samples with different offsets in double directions are displayed in Fig. 6. The offsets values for X-axis and Y-axis directions, expressed as (x, y), are (15.1, 16.1), (20.1, 19.8) and (25.7, 28.9) respectively, and the corresponding air-cavity length are ∼62.9, ∼61.2 and ∼60.6 μm, respectively.

In the strain sensitivity test, the fiber FP cavity device was mounted between two translation stages, of which one is fixed and the other is moveable, and the fiber is fixed by use of instant adhesive. The axial strain was introduced by controlling the translation stage and the range of strain produced was between 0 and 2000 $\mu\varepsilon$.

The reflection spectra and the output dip wavelength versus axial strain for the four device samples (A1 to A4) with single direction offsets of ∼15.1. ∼20.9 and ∼25.3 μm respectively, are displayed in Fig. 7. It can be seen from the figure that the dip wavelength experiences a red shift with the increase of axial strain, the dip wavelength and strain have a good linear relationship and the strain sensitivities obtained are 4.72, 5.51 and 6.37 pm/$\mu\varepsilon$ respectively. The fluctuations in the depth of dip wavelength are likely due to the uneven internal RI change of the cavity structure during the test. The cavity length, offset and strain sensitivity of the device samples are summarized in Table 1.

Fig. 8 demonstrate the reflection spectra and the output dip wavelength shift versus axial strain for three device samples (B$_1$ to B$_3$) with double direction offsets of (15.1, 16.1), (20.1, 19.8) and
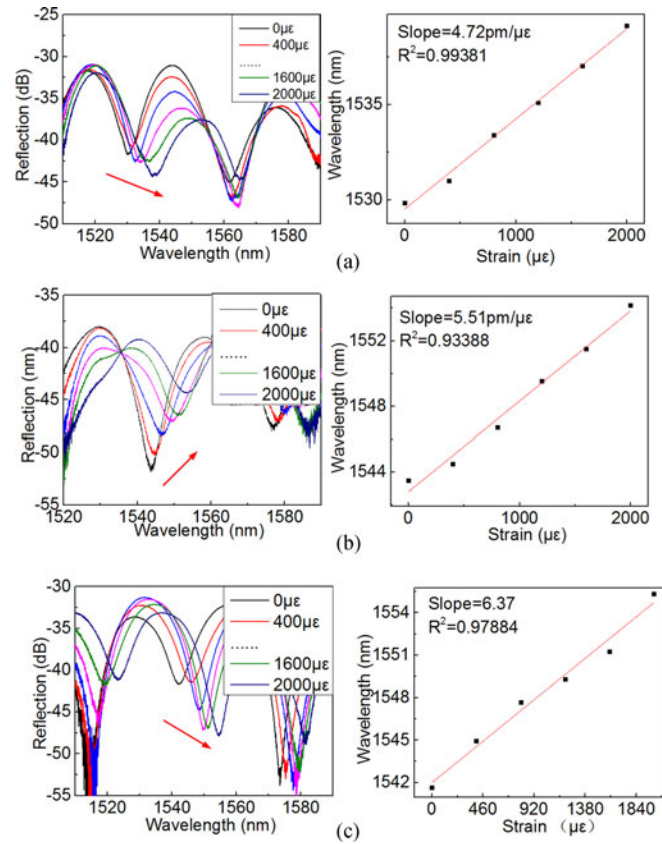
Fig. 7. The reflection spectra and the output dip wavelength versus axial strain for device sample with single direction offset of (a) ~15.1 μm, (b) ~20.9 μm and (c) ~25.3 μm.

TABLE 1

FP Cavity Sample Parameters

	L(μm)	O_1 (μm)	Sensitivity (pm/$\mu\varepsilon$)	The Linear Correlation Coefficient
A_1	62.5	15.1	4.72	0.99381
A_2	61.2	20.9	5.51	0.93388
A_3	60.7	25.3	6.37	0.97884

L stands for the cavity length, O_1 stands for the offset in single direction of the device sample.

(25.7, 28.9) respectively, with units in μm. It can be found from Fig. 8 that the output reflection spectrum of the device shifts toward longer wavelength when the axial strain is increased, and a good linear relationship can be obtained.

The highest sensitivity is achieved for sample B_3, when the offset in X and Y directions are ~25.7 and ~28.9 μm respectively. The cavity length, offset and strain sensitivity of the device samples are summarized in Table 2.

For comparison, the reflection spectra and the output dip wavelength versus axial strain for the FP cavity device sample without any offset and with cavity length of ~64.6 μm are displayed in
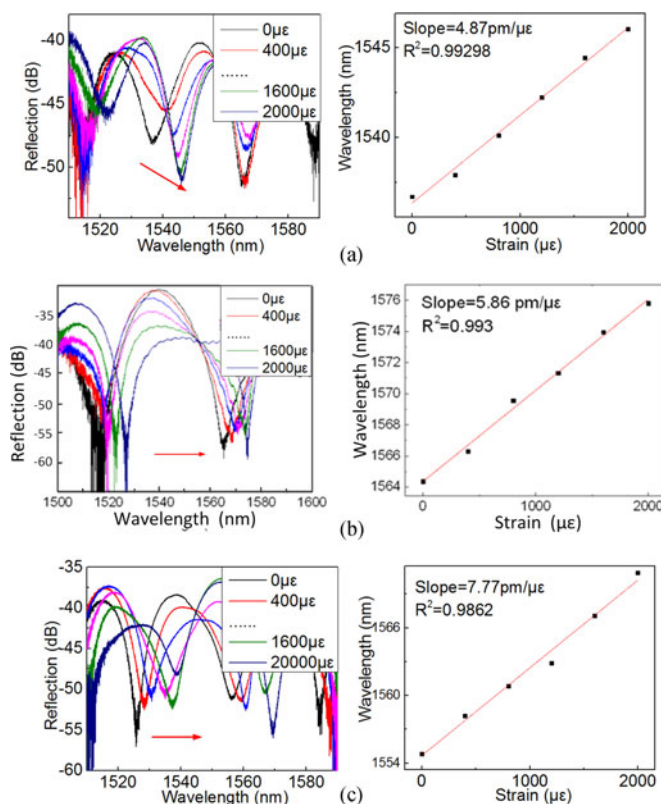
Fig. 8. The reflection spectra and the output dip wavelength versus axial strain for device sample with double direction offset of (a) (15.1, 16.1), (b) (20.1, 19.8) and (c) (25.7, 28.9), with units in μm.

TABLE 2
FP Cavity Sample Parameters

	L(μm)	O_1 (μm)	O_2 (μm)	Sensitivity (pm/$\mu\varepsilon$)	The linear correlation coefficient
B_1	62.9	15.1	16.1	4.87	0.99298
B_2	61.2	20.1	19.8	5.86	0.993
B_3	60.6	25.7	28.9	7.77	0.9862

L stands for the cavity length, O_1 and O_2 stand for the X and Y axis offsets of the device samples, respectively.

Fig. 9. The reflection spectra and relationship between dip wavelength and strain of the device are similar to that of the device with offset however, only $\sim$3.26 pm/$\mu\varepsilon$ is obtained, lower than most of the device samples with offset.

Thus, the strain sensitivity improvement achieved by adopting offset is $\sim$4.51 pm/$\mu\varepsilon$, for the inner air-cavity of similar value of cavity length.

In the reflection spectrums shown in Figs. 7–9, there are some small fluctuations, which lead that the spectrums are not smooth. This is mainly due to the uneven discharge in the process of fusion splicing of fiber with core offset.
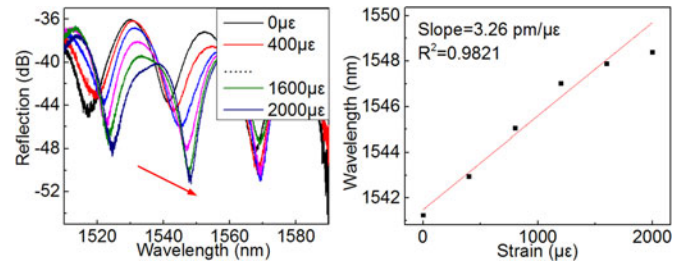
Fig. 9. The reflection spectra and the output dip wavelength versus axial strain for device sample without offset.
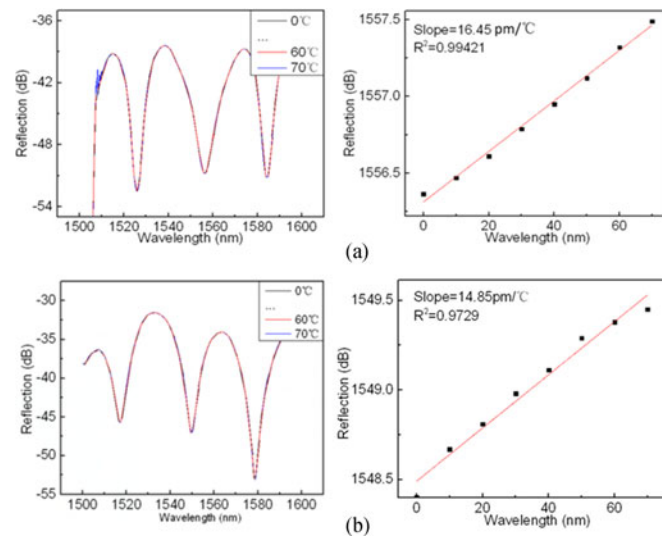

Fig. 10. The reflection spectra and the output dip wavelength versus temperature for device sample of (a) double direction offset of (25.7 μm, 28.9 μm), (b) single direction offset of ~25.3 μm.

When compared with the FPI based on inner air-cavity with small cavity wall thickness [14], our proposed device is more robust because of larger cavity wall thickness, and for those with ultra-thin cavity thickness [12], [13], our device has much larger cavity length, which allows easy observation of the reflection spectrum, hence facilitates the experiment implementation and improves the measurement accuracy.

The temperature responses of the FP cavity devices of different types are displayed in Fig. 10. The temperature sensitivities for a device sample with double direction offsets of (25.7 μm, 28.9 μm) is ~16.45 pm/°C, and the temperature sensitivities for device sample with single direction offset of ~25.3 μm is 14.85 pm/°C, respectively. Considering of their strain sensitivity of ~7.77, ~6.37 pm/$\mu\varepsilon$ respectively, the temperature cross-sensitivities are determined as ~2.12, ~2.33 $\mu\varepsilon$/°C respectively, which are lower than that of MZI(5.25 $\mu\varepsilon$/°C) [16] and PCF based Sagnac loop (175 $\mu\varepsilon$/°C [17].

4. Conclusion

In conclusion, we have successfully demonstrated an optical fiber FPI sensor based on inner air-cavity with high strain sensitivity. The inner air-cavity is fabricated by fusion splicing of two sections of etched MMF with offset. It is found that by introducing the offsets, the strain sensitivity can be greatly increased and in the case of introducing two dimensional offset, the strain sensitivity can

be increased by more than 4.5 pm/$\mu\varepsilon$. The device is simple in fabrication, robust in structure and economic in cost and has high potential in many strain sensing applications.

References

[1] X. Chen, F. Shen, Z. Wang, Z. Huang, and A. Wang, "Micro-air-gap based intrinsic Fabry–Perot interferometric fiber-optic sensor," *Appl. Opt.*, vol. 45, no. 30, pp. 7760–7766, Oct. 2006..

[2] E. Cibula and D. Donlagic, "In-line short cavity Fabry-Perot strain sensor for quasi distributed measurement utilizing standard OTDR," *Opt. Exp.*, vol. 15, no. 14, pp. 8719–8730, Jul. 2007.

[3] O. Frazao, S. H. Aref, J. M. Baptista, and J. L. Santos, "Fabry-perot cavity based on a suspended-core fiber for strain and temperature measurement," *IEEE Photon. Technol. Lett.*, vol. 21, no. 17, pp. 1229–1231, Sep. 2009.

[4] M. Deng, C.-P. Tang, T. Zhu, and Y. J. Rao, "PCF-based Fabry-Perot interferometric sensor for strain measurement at high temperature," *IEEE Photon. Technol. Lett.*, vol. 23, no. 30, pp. 700–702, Jun. 2011.

[5] S. Pevec and D. Donlagic, "All-fiber, long-active-length fabry-perot strain sensor," *Opt. Exp.*, vol. 19, no. 16, pp. 15641–15651, Aug. 2011.

[6] P. A. R. Tafulo, P. A. S. Jorge, J. L. Sandos, and O. Frazao, "Fabry-Perot cavities based on chemical etching for high temperature and strain measurement," *Opt. Commun.*, vol. 285, no. 6, pp. 1159–1162, 2012.

[7] D. W. Duan, Y. J. Rao, Y. S. Hou, and T. Zhu, "Microbubble based fiber-optic Fabry-Perot interferometer formed by fusion splicing single-mode fibers for strain measurement," *Appl. Opt.*, vol. 51, no. 8, pp. 1033–1026, Mar. 2012.

[8] V. R. Machavaram, R. A. Badcock, and G. F. Fernando, "Fabrication of intrinsic fibre Fabry-Perot sensors in silica fibres using hydrofluoric acid etching," *Sens. Actuators A*, vol. 138, no. 1, pp. 248–260, 2007.

[9] J. Zhang, G. D. Peng, L. Yuan, and W. Sun, "Composite-cavity-based Fabry-Perot interferometric strain sensors," *Opt. Lett.*, vol. 32, no. 13, pp. 1833–1835, Jul. 2007.

[10] B. H. Lee *et al.*, "Interferometric fiber optic sensors," *Sensors*, vol. 12, no. 3, pp. 2467–2486, 2012.

[11] F. C. Favero, L. Araujo, G. Bouwmans, V. Finazzi, J. Villatoro, and V. Pruneri, "Spheroidal Fabry-Perot microcavities in optical fibers for high-sensitivity sensing," *Opt. Exp.*, vol. 20, no. 7, pp. 7112–7118, Mar. 2012.

[12] M. S. Ferreira, J. Bierlich, J. Kobelke, K. Schuster, J. L. Santos, and O. Frazão, "Towards the control of highly sensitive Fabry-Perot strain sensor based on hollow-core ring photonic crystal fiber," *Opt. Exp.*, vol. 20, no. 20, pp. 21946–21952, Sep. 2012.

[13] Y. Zhao, M.-Q. Chen, R.-Q. Lv, and F. Xia, "In-fiber rectangular air Fabry-Perot strain sensor based on high-precision fiber cutting platform," *Opt. Commun.*, vol. 384, pp. 107–110, 2017.

[14] S. Liu *et al.*, "High-sensitivity strain sensor based on in-fiber rectangular air bubble," *Sci. Rep.*, vol. 5, 2015, Art. no. 7624.

[15] Y. Liu, D. N. Wang, and W. P. Chen, "Crescent shaped Fabry-Perot fiber cavity for ultra-sensitive strain measurement," *Sci. Rep.*, vol. 6, 2016, Art. no. 38390.

[16] B. Wang *et al.*, "Mach–Zehnder interferometer based on interference of selective high-order core modes," *IEEE Photon. Technol. Lett.*, vol. 28, no. 1, pp. 71–74, Jan. 2016.

[17] H. Gong, C. C. Chan, L. Chen, and X. Dong, "Strain sensor realized by using low-birefringence photonic-crystal-fiber-based sagnac loop," *IEEE Photon. Technol. Lett.*, vol. 22, no. 16, pp. 1238–1240, Aug. 2010.